Atmospheric Science Letters

RMetS Royal Meteorological Society

RESEARCH ARTICLE OPEN ACCESS

How Well Is the Lake-Land Breeze Circulation of Lake Victoria Captured in ECMWF Operational Analysis?

Musa Ssemujju[1,2] | Marlon Maranan[1] | Andreas H. Fink[1] | Simon Ageet[1]

[1]Institute of Meteorology and Climate Research Troposphere Research (IMKTRO), Karlsruhe Institute of Technology (KIT), Karlsruhe, Germany | [2]Uganda Department of Meteorological Services (UDMS), Ministry of Water and Environment, Kampala, Uganda

Correspondence: Musa Ssemujju (musa.ssemujju@kit.edu; semujjumusa@yahoo.com)

Received: 3 June 2026 | **Revised:** 19 July 2026 | **Accepted:** 28 July 2026

Keywords: detection algorithm | Lake Victoria | land-lake-breezes | operational analysis

ABSTRACT

Lake-breeze fronts (LBFs) are important drivers of cloudiness, deep moist convection, and heavy precipitation around large tropical lakes, yet their representation in global forecast systems remains poorly understood. This study evaluates the ability of the ECMWF Integrated Forecasting System (IFS) 9 km operational analyses to represent the lake-breeze system over the Lake Victoria basin in Uganda during December–February and June–August 2017–2022. A recently developed objective lake-breeze detection algorithm (OLBDA) is applied to hourly station data and IFS surface data to identify LBF passages. Results show that while the IFS captures the coherent progression of the LBF from early to late afternoon, the analysis reveals biases, including an overprediction of LBF occurrence by ~26% and an early arrival of 1–2 h at most stations. Among three commonly used parameters to delineate LBFs, that is, surface convergence, and gradients of surface specific humidity and boundary-layer height (BLH), the latter two emerge as the most reliable indicators of LBF structure and evolution. Composite and vertical cross-section analyses reveal physically consistent three-dimensional lake-breeze features in the IFS, yet contrasts occur between western and northern transects. The NW-SE transect shows stronger vertical motion and deeper inland penetration when compared to the North–South transect. The latter is likely related to the mean easterly low-level flow over the lake. The depth of the BLH in the late afternoon is 3 km. Overall, our results suggest that ECMWF IFS operational analyses can be reliably used to study lake-breeze systems in both observational and modeling contexts.

1 | Introduction

Lake-breeze fronts (LBFs) are key components of coastal mesoscale meteorology that arise from diurnal lake-land thermal contrasts and strongly modulate boundary-layer structure, low-level convergence, convection, local air quality, and pollutant transport (Papanastasiou and Melas 2009; Crosman and Horel 2010; Sills et al. 2011; Fu et al. 2021). Despite their importance, accurate representation of LBFs in global numerical models and reanalysis products remains challenging due to their small horizontal scale (typically ~1–10 km), sharp surface gradients, and strong dependence on lake geometry, synoptic background flow, and surface fluxes (Laird et al. 2001; Hannak et al. 2017). The operational analysis from the European Centre for Medium-Range Weather Forecasts (ECMWF) Integrated Forecasting System (henceforth called IFS) has been available at 9 km since 2016 (ECMWF 2016), thus should, in principle, be able to reproduce mesoscale features such as LBFs. If this can be proven, IFS can be used to study individual cases and climatological characteristics of lake-land breeze (LLB) systems as well as serve as initial and boundary conditions for model studies at higher spatial resolutions. This is particularly relevant in sea and lake shores with poor surface and upper-air station density.

Over Lake Victoria (Figure 1), the second largest freshwater lake on Earth, numerous studies have examined the environmental

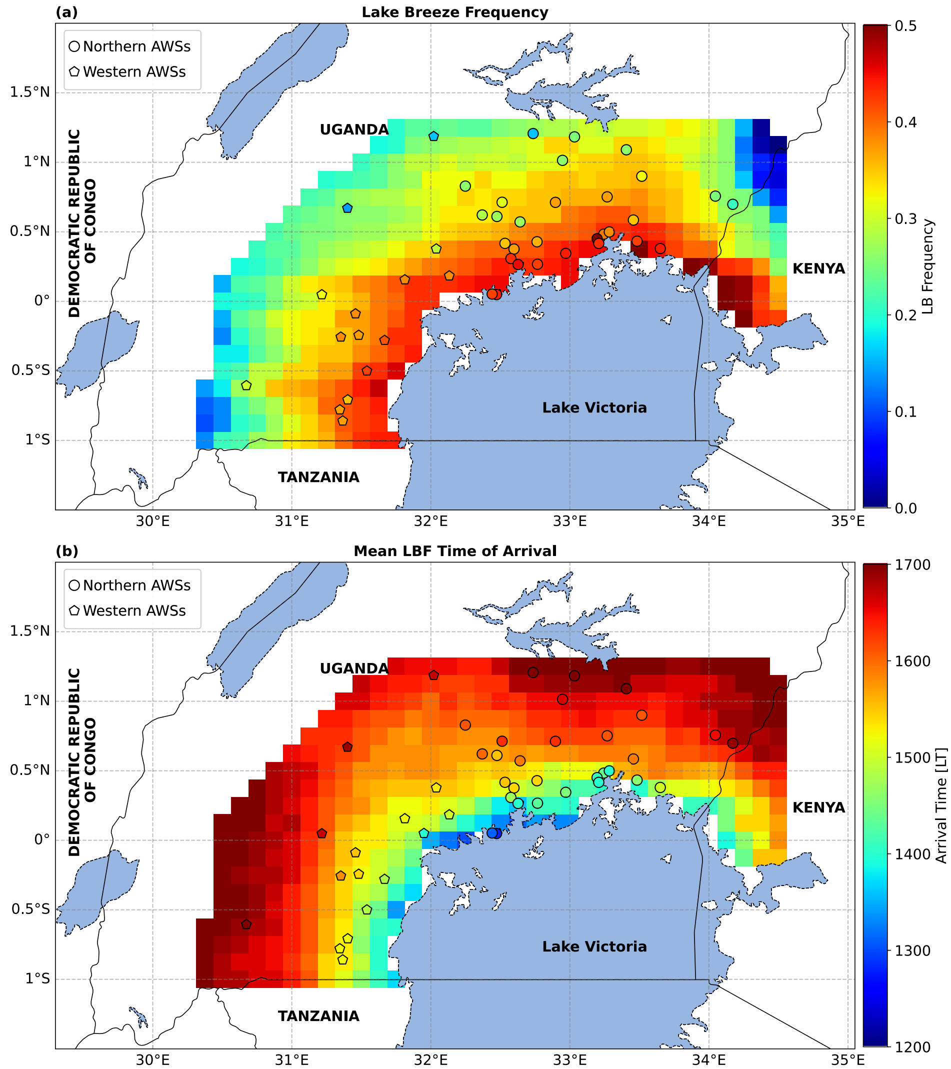

FIGURE 1 | A comparison of IFS (grids) and AWSs (scatters) regarding (a) lake-breeze frequency and (b) mean time of arrival (LT) for the dry months of DJF and JJA during 2017–2022. The colored pixels show the study region. Northern and western AWSs are denoted by circle and pentagon markers, respectively.

controls on precipitation extremes and severe thunderstorms in the Lake Victoria Basin (e.g., Chamberlain et al. 2014; Thiery et al. 2016; Woodhams et al. 2019; Finney et al. 2020). A key mechanism identified is the land-lake temperature contrast, which drives the Lake Victoria LLB circulation and plays a fundamental role in the initiation and organization of convection (e.g., Flohn and Fraedrich 1966; Anyah et al. 2006; Thiery et al. 2015; Van de Walle et al. 2020). These LLBs typically develop during the afternoon as the surrounding land heats more rapidly than the lake surface, generating onshore flow that converges over and around the lake (Virts and Goodman 2020). The LLB circulations are the primary control on the timing, location, and propagation of convective storms over the basin (Woodhams et al. 2019). Because these mesoscale circulations occur on spatial scales of only a few kilometers, their representation is highly sensitive to model resolution. Previous studies have demonstrated that convection-permitting models can realistically reproduce the observed structure and diurnal evolution of Lake Victoria lake-breezes and associated thunderstorms (e.g., Woodhams et al. 2019, 2022; Finney et al. 2020). In contrast, global forecasting systems such as the ECMWF IFS operate at resolutions that may not fully resolve the detailed dynamics of the lake-breeze circulation, instead relying partly on parameterized representations of convection and other sub-grid-scale processes. The performance of such models in coastal and lake-influenced environments is known to be highly sensitive to the representation of boundary-layer mixing, near-surface thermodynamics, and lake-land thermal contrasts (Holtslag et al. 2013; Savazzi et al. 2022), raising questions about how effectively LLBs can be captured at coarse resolution. Despite the well-established role of LLBs in controlling convective initiation, organization, and propagation over Lake Victoria, the extent to which these features are represented in global forecasting systems remains largely unquantified in literature. This gap is particularly important because IFS-based forecasts and reanalyses underpin a wide range of weather and climate applications (Hersbach et al. 2020; Brown et al. 2026), and are frequently relied upon for operational forecasting and atmospheric research in observation-sparse regions such as the Lake Victoria basin.

In the present study, we take the unique opportunity to evaluate IFS with respect to its ability to represent the LLB circulation over Lake Victoria in East Africa. Building upon the methodology and findings in Ssemujju et al. (2026), in which the Objective Lake Breeze Detection Algorithm (OLBDA) was developed and validated using a dense surface station network, we extend this line of research by applying the algorithm to hourly ECMWF IFS operational analysis, therein treating model grid points as pseudo-stations. This approach provides a spatially continuous diagnosis of LBF occurrence, position, geometry, timing, and propagation speed, thereby overcoming the spatial limitations of relatively sparse point-based surface observations. Using the previously established lake-breeze day catalog as an observational benchmark, we quantitatively assess, for the first time, the ability of IFS to reproduce the occurrence, timing, inland propagation, and three-dimensional meteorological characteristics of LBFs over Lake Victoria. This evaluation provides new insight into the skill of the IFS in representing the full evolution of the lake-breeze circulation, including aspects that cannot be diagnosed from surface point observations alone. Finally, using the detected fronts as a reference, we assess three computationally simple, physically motivated proxy variables to determine whether standard IFS output fields provide consistent and interpretable indicators of lake-breeze activity relevant for forecasting over Lake Victoria.

2 | Data and Methods

2.1 | Data

This study uses hourly output from the ECMWF IFS Cycles 43–47 operational forecast dataset (ECMWF 2017, 2019, 2020, 2022). The data are provided at 9 km horizontal resolution and are available at the surface and across 137 model levels, enabling a consistent analysis of surface and boundary-layer processes relevant to lake-breeze dynamics. The analysis is conducted over the northern shores of Lake Victoria, Uganda, during the dry seasons of December–February (DJF) and June–August (JJA) over the period 2017–2022, consistent with Ssemujju et al. (2026).

We utilize surface variables including 2-m temperature, 2-m dewpoint temperature, 10-m wind components, surface pressure, as well as boundary-layer height. Specific humidity is computed from 2-m dewpoint temperature and surface pressure using the MetPy Python package (v1.7; May et al. 2019). Additionally, hourly vertical velocity, temperature, and horizontal wind components are extracted for the lowest 38 model levels, extending to ~5 km above ground level (AGL).

For validation of LBFs detected in IFS analyses, we use hourly surface observations obtained from a network of 45 automatic weather stations (AWSs; Figure 1) operated by the Trans-African Hydrometeorological Observatory (TAHMO; van de Giesen et al. 2014) and the Uganda Department of Meteorological Services (UDMS). In addition, satellite visible imagery from NASA's Earth Observing System Data and Information System (EOSDIS) Worldview platform is used. Here, lake-breeze and non-lake-breeze days identified from satellite visible imagery serve as the reference dataset for validating IFS-detected lake-breeze days, following the methodology of Ssemujju et al. (2026).

2.2 | LBF Identification Using OLBDA

LBF passages are objectively identified using the OLBDA, which detects characteristic thermodynamic and kinematic signatures of the lake breeze at individual stations or grid points within the study domain. The algorithm is applied to hourly grid point values of wind and temperature between 09:00 and 19:00 LT (daylight hours) to determine frontal location and occurrence. At a given station, the algorithm follows a sequential procedure by checking for the increase of the magnitude of onshore winds, a sharp decrease in temperature, and an increase in humidity or dew point (Sills et al. 2011; Miller et al. 2003). Finally, the algorithm applies a precipitation criterion to exclude the possibility of a convective cold pool-driven impact on the onshore wind. By doing this, the algorithm ensures that all the changes in the measured meteorological parameters are exclusively produced by the lake-breeze frontal passages. If all these criteria flags are passed sequentially, then the LBF passage at that station is counted. The OLBDA algorithm identifies LBF passages by adopting the threshold criterion of Ssemujju et al. (2026) based on the lowest 30% of temperature drops and the highest 30% of dewpoint and wind speed increases, but on a 1-h timescale to accommodate for the native temporal resolution of IFS. This way, we maintain methodological consistency with the observational framework and ensure that differences between the observed and simulated lake-breeze characteristics reflect the performance of the IFS analysis rather than changes in the event detection criteria. We refer to Ssemujju et al. (2026) for full methodological details on OLBDA.

2.3 | Definition of a Lake-Breeze Day and Performance of OLBDA

Following Ssemujju et al. (2026), and accounting for the limited number of coastal AWSs, a lake-breeze day in the station dataset is defined as a day on which the OLBDA detects LBF passage in at least three coastal stations. We apply a similar approach to IFS by treating the nearest IFS grid points as stations and then checking whether at least three of these pseudo-coastal stations recorded a passage. This ensures a consistent and fair comparison of lake-breeze day detection between the AWS and IFS datasets. The performance of the OLBDA when applied to IFS analysis is then evaluated using the same methodology and reference dataset of the manually identified satellite lake-breeze and non-lake-breeze days as in Ssemujju et al. (2026). Furthermore, for each station, lake-breeze days detected by the OLBDA in the ECMWF IFS analysis were matched with the corresponding lake-breeze days identified from the AWS observations at the same location. Frequency bias was then calculated as the difference between the number of lake-breeze days detected in the IFS and AWS datasets, whereas arrival-time bias was calculated as the difference between the times of first LBF arrival in the two datasets for matched events. Event occurrence statistics and arrival time biases were computed consistently across the full network of 45 AWS surface stations and for all days when stations recorded observations.

2.4 | Identifying LBFs Using Proxy Fields in IFS

Global reanalysis and forecast systems such as the IFS provide spatially continuous, three-dimensional fields of winds, moisture, and boundary-layer structure beyond the capabilities of surface stations. If the OLBDA framework can robustly identify LBFs from gridded IFS output using near-surface wind, temperature, and dewpoint, then the full model state can be exploited to evaluate additional physically motivated diagnostics of LBF activity.

To assess the suitability of such diagnostics, we evaluate three commonly used proxies between 09:00 and 19:00 LT: the horizontal gradient of boundary-layer height (∇BLH; Antonelli and Rotunno 2007; Kalthoff et al. 2020), low-level horizontal wind convergence ($-\nabla . U$; Miller et al. 2003; Drobinski et al. 2006; Crosman and Horel 2010; Brown et al. 2026), and the horizontal gradient of specific humidity (∇q; Borne et al. 1998; Laird et al. 2001; Zhu and Atkinson 2004; Brown et al. 2026). Together, these diagnostics leverage the spatial and vertical structure of IFS fields to assess whether the model captures robust mesoscale signatures of LBFs.

3 | Results and Discussion

3.1 | LBF Occurrence Frequency

Using the lake-breeze day definition in Section 2.3, the OLBDA identifies 526 and 417 lake-breeze days in the IFS and AWS datasets, respectively, out of 1093 DJF and JJA days within the 2017–2022 study period, corresponding to 48% and 38% (Table 1; Figure 1). Of these, 400 are common to both datasets, meaning that 126 and 17 detected lake-breeze days are exclusive to IFS and AWS, respectively. When applied to IFS, the OLBDA achieves a probability of detection of 0.71 and a false alarm ratio of 0.25, which are comparable to the corresponding AWS scores of 0.68 and 0.20, respectively. In IFS, lake-breeze days are nearly evenly distributed between the western and northern sectors, whereas AWS observations show higher frequency in the northern sector. Interannual variability is consistent across datasets, with 2021 (2018) recording the highest (lowest) lake-breeze days (Table 1).

Figure 1a shows that both datasets exhibit a coherent spatial gradient, with the highest LBF occurrences concentrated along the Lake Victoria shoreline and progressively decreasing inland. This pattern is consistent with the expected spatial footprint of LBFs, frequent near the lake where the circulation forms, and diminishing inland as the temperature-driven pressure gradient weakens.

The IFS reproduces this large-scale pattern but exhibits a systematic positive bias in LBF frequency. Across all stations, 30 of 45 (~67%) show higher LBF frequencies in the IFS than in the AWS, suggesting that the model overestimates LBF occurrence. This positive bias is typically ~5% and spatially consistent, with 10 of 15 (~67%) stations in the western and 20 of 30 (~67%) in the northern sector. The overestimation is most pronounced within ~20 km of the shoreline, where occurrence frequencies reach ~50% in both datasets but decline more slowly inland in the IFS than in the AWSs. On average, LBF frequency in IFS decreases by ~4% every 20 km inland compared to a steeper decline of ~6% in AWS data.

The positive bias in occurrence frequency in IFS extends even to the most distant stations, with 4 of 7 showing higher LBF frequencies than in AWS. This suggests that the LBF in the IFS model propagates farther and more frequently inland than observed. This behavior may reflect an excessively smooth or overly persistent representation of the lake-land temperature contrast in the IFS, which can effectively strengthen or sustain the thermal gradient that drives LBF initiation and inland penetration. It may also stem from unresolved sub-grid processes such as shoreline roughness transitions, small-scale topographic variations, local land-use heterogeneity, or shallow boundary-layer

TABLE 1 | Summary of lake-breeze days statistics in December–February and June–August (DJF-JJA) during 2017–2022 for IFS model (collocated grid points) and AWS observations.

	Percentage of days in DJF and JJA (182 days) with lake-breezes across both sites		Number of days on Western coast with lake-breezes		Number of days on Northern coast with lake-breezes		Number of days extra in IFS model compared to AWS		Excess IFS detection as a percentage of total days sampled (182 days)		OLBDA performance: Probability of detection		OLBDA performance: False alarm ratio	
Year	**IFS**	**AWS**	**IFS**	**AWS**	**IFS**	**AWS**	**West**	**North**	**West**	**North**	**IFS**	**AWS**	**IFS**	**AWS**
2017	49%	38%	69	50	70	62	19	8	10%	4%	0.69	0.65	0.21	0.19
2018	37%	29%	66	42	55	41	24	14	13%	8%	0.61	0.56	0.22	0.19
2019	41%	32%	71	55	62	56	16	6	9%	3%	0.66	0.59	0.19	0.17
2020	47%	40%	80	72	70	70	8	0	4%	0%	0.69	0.67	0.20	0.18
2021	62%	46%	84	84	105	88	0	17	0%	9%	0.80	0.80	0.35	0.22
2022	53%	44%	83	75	92	75	8	17	4%	9%	0.82	0.83	0.32	0.23
Mean	48%	38%	76	63	76	65	13	10	7%	6%	0.71	0.68	0.25	0.20

Note: West and North represent western and northern sectors of the lake, respectively.

mixing that in reality inhibit inland penetration of the breeze. However, along portions of the northern coast, the IFS closely matches observed coastal frequencies and reproduces the inland decline to ~20% within ~40 km. Overall, the IFS captures the regional-scale spatial gradient of LBF occurrence but systematically overestimates event frequency.

3.2 | Mean Time of LBF Arrival

Figure 1b presents the mean LBF arrival time from AWSs and IFS grid points. The mean arrival times show a clear and coherent inland progression, with earlier arrivals (12:00–14:00 LT) near the lakeshore and later arrivals (16:00–17:00 LT) farther inland, consistent with the expected daytime propagation of the LBF seen in previous work (e.g., Anyah et al. 2006; Chamberlain et al. 2014; Woodhams et al. 2019; Ssemujju et al. 2026). Both datasets capture this distance-dependent delay, indicating realistic representation of inland progression.

The IFS, however, exhibits an early-arrival bias. Across the network, 27 of 45 stations (~60%) record LBF arrivals at least 1 h earlier than observed. Of the remaining stations, 11 (~24%) show delayed arrivals, while the rest agree closely. The bias is strongest in the western sector, where 12 of 15 stations (80%) record earlier arrival, compared to 15 of 30 (50%) in the northern sector. On average, IFS leads observations by ~1 h, with local leads of 1–2 h depending on the station. It should be noted that the early-arrival bias occurs when averaged over all LBF days. In fact, late arrivals are frequently detected as well, as seen in the comparison of LBF arrival times between IFS and AWSs in Figure S1.

Despite this bias, spatial patterns are consistent across datasets. In the IFS, LBFs typically arrive first along the northern coast (~12:00 LT) and then along the western coast (~13:00 LT), slightly earlier than observed but following the same sequence. This shows that the tendency of the IFS analysis to simulate earlier arrival times is consistent across all geographic sectors of the study region, with only slight variations in the average lead time of the simulated fronts. Although the causes of this earlier onset and the faster, deeper inland propagation of the LBF remain uncertain, they likely reflect a too rapid generation of lake-land thermal contrasts, thereby promoting earlier initiation and accelerated inland propagation of the LBF.

3.3 | Performance of Diagnostic Proxy Variables From IFS: Case Study of 26 January 2022

To evaluate the proxy variables described in Section 2.4, we examine a representative lake-breeze case on 26 January 2022. This day was consistently identified as a lake-breeze day by satellite imagery and the OLBDA across most AWS stations and IFS grid points, with clearly defined frontal progression. Figure 2 compares the diurnal evolution of the LBF inferred from these proxies with OLBDA- and satellite-inferred frontal positions at 12, 15, and 18 LT. All three LBF metrics exhibit coherent inland propagation. At 12 LT, a clear signal delineating the shoreline appears in all three fields, indicating the initial development of a lake-driven circulation (Figure 2a,d,g). By 15 LT, this signal intensifies and extends inland, consistent with the daytime progression of a developing lake-breeze system (Figure 2b,e,h), while by 18 LT (Figure 2c,f,i) the signal becomes more diffuse and further displaced inland.

However, among the three diagnostics, ∇BLH provides the most continuous and well-defined frontal signature throughout the day (Figure 2a–c). At 12 LT, strong land-lake contrasts in boundary-layer depth produce a pronounced ∇BLH signal that becomes more organized by 15 LT and remains identifiable, though weaker, by 18 LT. The resulting narrow and spatially coherent band allows the front to be tracked from initiation through inland propagation. The ∇q also delineates the LBF clearly, particularly during the early-to-mid afternoon (Figure 2d–f). A sharp ∇q band forms along the shoreline at 12 LT, intensifies and advances inland by 15 LT, and remains detectable at 18 LT, albeit broader and less sharply defined than ∇BLH. Overall, ∇q appears a suitable diagnostic, but tends to develop other strong gradient structures between the LBF and the shoreline (Figure 2e,f). In contrast, horizontal convergence exhibits weaker and more fragmented signatures (Figure 2g–i), with broader and less spatially consistent bands near the shoreline than those identified by ∇BLH and ∇q. It should be noted that, although IFS exhibits an overall tendency for faster LBF propagation when averaged across all identified lake-breeze days (Figure 1b), Figure 2 represents a single case study in which the observed front (blue line) propagates faster than the IFS-derived front (red line) in some areas. Such event-to-event variability is expected and does not contradict the statistical results presented in the previous section, which are based on the complete lake-breeze-day dataset.

As a quantitative validation of the frontal locations, satellite imagery from Terra-MODIS (10:30 LT), NOAA-20 (12:20 LT) and Suomi-NPP (13:30 LT) are shown in Figure 2j–l. In both scenes, cloud lines or sharp surface reflectance contrasts align closely with fronts identified by ∇BLH and ∇q, providing independent confirmation of these diagnostics in this region. This visual agreement supports both diagnostics as physically consistent indicators of LBF position and morphology. Thus, LBF climatologies from IFS ∇BLH and ∇q will be henceforth considered.

3.4 | Composite of LBF Propagation Within ∇BLH and ∇q

To further assess the robustness of the two best-performing diagnostics, Figure 3 presents composites of ∇BLH and ∇q for 400 common lake-breeze days, providing a generalized view of how well these fields capture the typical evolution of the observed LBF. Before noon, developing lake-land thermal contrasts produce weak, spatially incoherent gradients in both ∇BLH and ∇q. Consistent with surface observations, no shoreline-anchored front is evident, as a coherent LBF forms only after ~12 LT. We therefore focus our analysis from 12 LT onward.

At 12 LT, both ∇BLH and ∇q show gradient maxima closely aligned with the OLBDA-derived front along most shoreline sectors (Figure 3a,d). The close agreement in frontal position, curvature and shoreline-parallel orientation indicates that both proxies reliably capture the early-stage LBF structure despite substantial event-to-event variability.

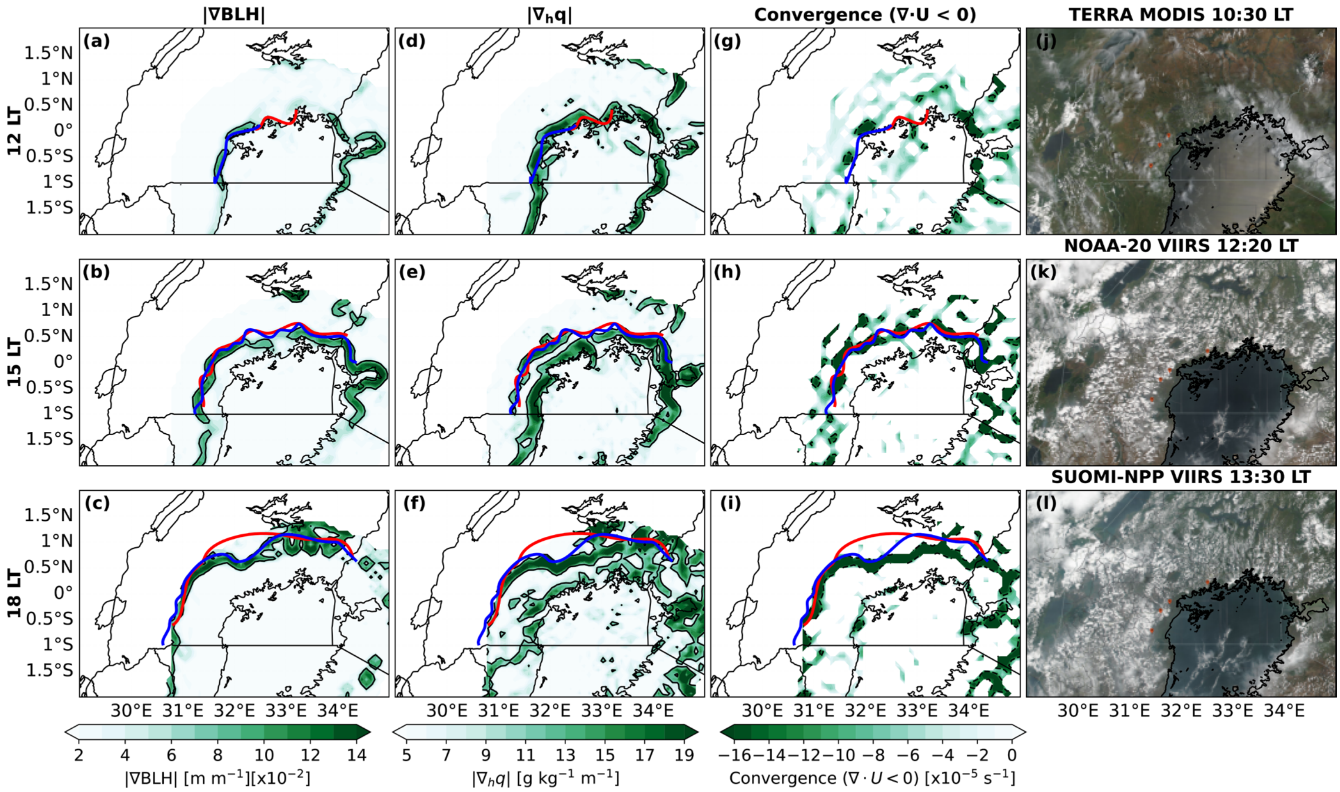

FIGURE 2 | Comparison of three proxy diagnostics for identifying the lake-breeze front (LBF) in the IFS on 26 January 2022 at 12 (top row), 15 (middle row), and 18 LT (bottom row). Shown are (a–c) boundary-layer height gradient (∇BLH), (d–f) horizontal gradient of specific humidity (∇q), and (g–i) low-level horizontal convergence. Panels (j–l) show corresponding satellite imagery from MODIS Terra (10:30 LT), VIIRS NOAA-20 (12:20 LT), and VIIRS Suomi-NPP (13:30 LT), respectively, for visual comparison of observed frontal position. Red and blue lines indicate LBF position identified by the OLBDA in AWS and IFS data, respectively, for this case study. The black contours delineate areas where the threshold values applied to the proxy-variable fields are exceeded: $\nabla BLH > 0.07\,\mathrm{m\,m^{-1}}$, $\nabla q > 10\,\mathrm{g\,kg^{-1}\,m^{-1}}$, and convergence $< -12\times10^{-5}\,\mathrm{s^{-1}}$.

From 12 to 18 LT, both fields track the observed inland propagation of the breeze but differ structurally. The ∇BLH field provides the most intuitive correspondence, with gradient bands advancing inland in parallel with the OLBDA-detected front and retaining a compact structure that closely matches the observed frontal geometry (Figure 3a–c). In contrast, ∇q signal expands inland rather than forming a single sharp boundary, especially in the western sector, where coherent, narrow contours are less prominent (Figure 3d–f). Here, agreement with observations is better reflected in the inland extent and spatial footprint of enhanced ∇q than in a discrete moving front.

Despite these structural differences, both diagnostics retain strong spatial correspondence with the observed front throughout the afternoon. The ∇q reliably highlights the moisture discontinuity associated with the breeze, while ∇BLH more clearly delineates a migrating frontal boundary. This consistency relative to the OLBDA-identified front demonstrates that ∇BLH and ∇q are reliable and complementary proxies for diagnosing LBF structure and propagation in the IFS.

3.5 | Vertical Structure and Evolution of the Lake-Breeze Circulation (LBC)

The almost complete lack of upper-air observations inhibits any in situ studies on the vertical structure of the LBF during the course of the day. Based on the reasonable delineation of the LBF by IFS, we created daytime composite cross-sections of vertical velocity (w), BLH, and virtual potential temperature (θ_v) along transects perpendicular to the western and northern shores (Figure 4a) to examine the diurnal vertical structure.

The vertical cross-sections reveal a well-defined thermally-driven LBC evolving systematically from 12 to 18 LT (Figure 4b–g). At 12 LT, a shallow ascent zone (orange shading) forms near the shoreline along both transects, indicating the lake-breeze initiation (Figure 4b,e). Over the lake, stable stratification maintains a shallow boundary layer (black line), while inland heating drives boundary-layer growth. A modest cross-shore θ_v gradient (green contours) establishes the thermal contrast required for circulation development, and weak low-level onshore flow emerges but remains confined near the coast. This structure is consistent with the initial adjustment phase of thermally-forced breezes described in classical conceptual models (Simpson 1994).

By 15 LT, the circulation peaks (Figure 4c,f). A pronounced ascent zone develops tens of kilometers inland, collocated with the inland-most extent of onshore flow, representing the LBF. The strongest ascent coincides with a sharp BLH gradient, indicating low-level convergence, intrusion of cooler lake-modified air, and frontal lifting characteristic of a density-current head. Ahead of the front, strong surface heating rapidly deepens the

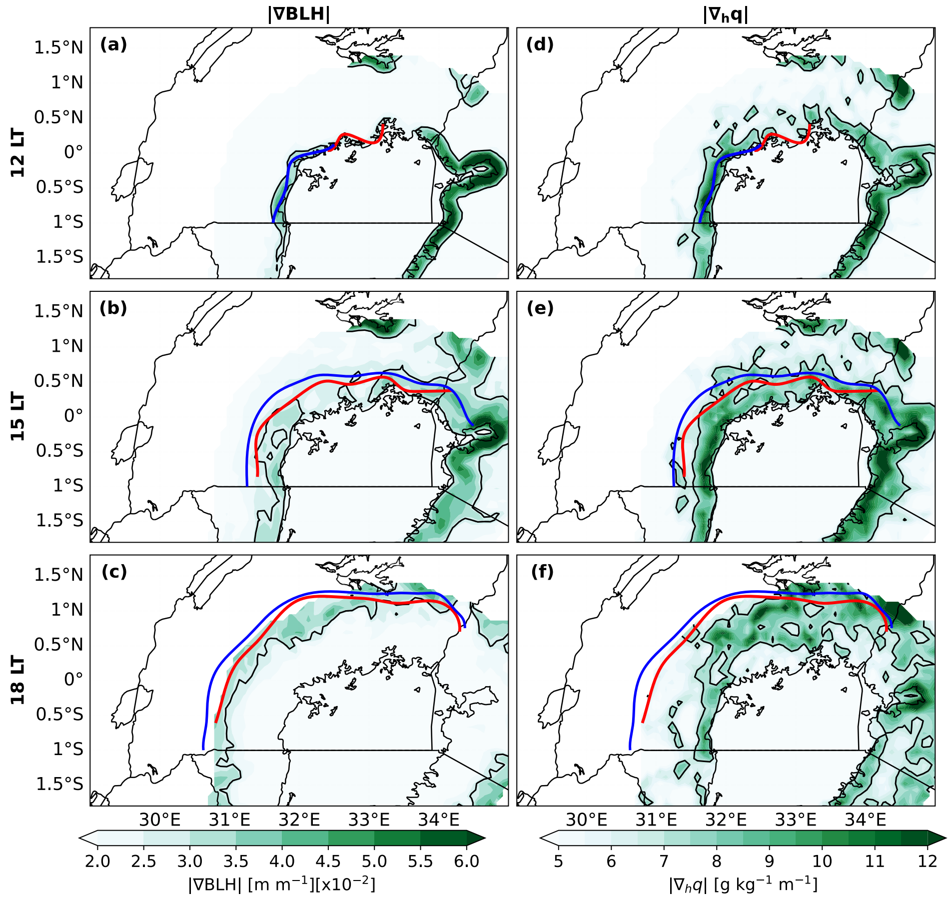

FIGURE 3 | Composite lake-breeze structure derived from all satellite-identified lake-breeze days, shown for (a–c) boundary-layer height gradient (∇BLH), and (d–f) horizontal gradient of specific humidity (∇q) at 12 (top row), 15 (middle row), and 18 LT (bottom row). Red and blue lines indicate LBF position identified by the OLBDA in AWS and IFS data, respectively. The black contours delineate areas where the threshold values applied to the proxy-variable fields are exceeded: $\nabla BLH > 0.028\,\mathrm{m\,m^{-1}}$, and $\nabla q > 7\,\mathrm{g\,kg^{-1}\,m^{-1}}$.

boundary-layer, leading to enhanced mixed-layer growth inland. The inland, weakly stratified and well-mixed boundary-layer reaches a maximum depth of ~3 km AGL, consistent with previous studies over Lake Victoria (Fraedrich 1968; Woodhams et al. 2019), and within the typical 2–3 km depth of vigorously convective boundary layers under strong surface heating (e.g., Stull 1988; Miller et al. 2003). Streamlines indicate a fully developed closed circulation cell with well-defined onshore flow feeding the frontal ascent and a distinct return branch aloft, while weakened vertical θ_v gradients inland indicate increased instability and continued deepening of the mixed layer relative to the cooler, more stably stratified lake-modified air.

By 18 LT, the circulation weakens as surface heating diminishes (Figure 4d,g). Frontal ascent becomes shallower and less coherent, the onshore flow retracts toward the shoreline, and thermal gradients relax. The inland BLH decreases and the frontal gradient becomes less distinct, marking a transition to the decay phase. Residual ascent persists longer along the western transect, but overall vertical motion diminishes, consistent with the canonical diurnal cycle of thermally driven breezes.

Despite similar evolution, the two transects differ systematically. Along the western transect (Figure 4e–g), ascent is deeper and stronger, boundary-layer growth is more rapid, and the LBF penetrates farther inland (~200 km), with a clearer return flow aloft. Along the northern transect (Figure 4b–d), ascent is weaker, boundary-layer development is more gradual, and inland penetration is limited (~130 km). These contrasts reflect shoreline orientation relative to the prevailing easterlies (see supporting information in Ssemujju et al. 2026). Along the western shore, the easterlies impinge more perpendicular to the coast, enhancing low-level convergence and strengthening frontal lifting, whereas along the northern shore, more parallel flow weakens convergence and yields a weaker LBF. Similar sensitivities to synoptic wind alignment have been documented in previous lake- and sea-breeze studies (e.g., Simpson 1994; Miller et al. 2003; Markowski and Richardson 2010).

Overall, the coupled evolution of w, BLH, and θ_v demonstrates a classic thermally-driven mesoscale circulation whose strength, vertical extent, and inland propagation are strongly governed by surface heating and modulated by synoptic flow orientation. This three-dimensional analysis further highlights the advantage of the IFS data by revealing aspects of the LBF that cannot be resolved from a two-dimensional perspective, including the vertical thermodynamic structure of the front, the return flow aloft, the pronounced BLH gradient marking the frontal boundary, and variations in boundary-layer depth throughout the evolution of the lake breeze. These results reinforce established LBC theory while providing new insight into its vertical structure and asymmetry over Lake Victoria.

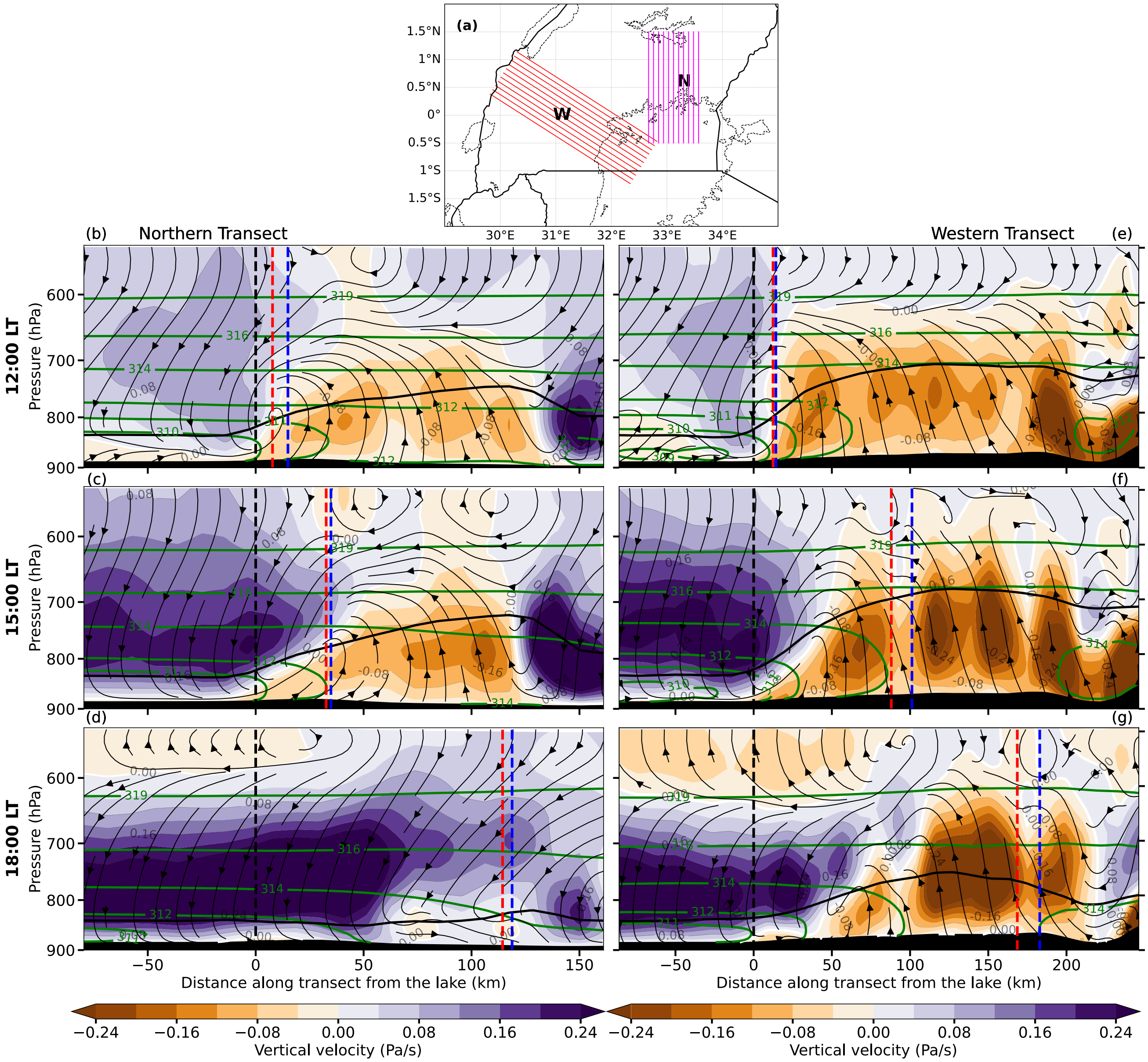

FIGURE 4 | (a) Study domain showing red and magenta lines (transects) oriented perpendicular to the western (W) and northern (N) shores of Lake Victoria, respectively, used to compute the mean cross-sections. (b)–(d) and (e)–(g) Composite vertical cross-sections of vertical motion along the northern and western transects at 12:00 (top row), 15:00 (middle row), and 18:00 LT (bottom row), respectively. Shading denotes vertical velocity (orange = ascent, purple = descent). The black solid line shows the boundary layer height, green contours represent virtual potential temperature, and arrows indicate 2-D streamline flow. The red and blue dashed vertical lines in (b)–(g) roughly mark the composited LBF location from AWS and IFS, respectively, along the averaged northern and western transects. Distance in km is measured from the lake shoreline (vertical dashed black line) with positive (negative) values showing distance away from (into) the lake.

4 | Summary and Conclusions

This study evaluates how well LBFs are represented in ECMWF IFS operational forecasts over the Lake Victoria region. Applying the OLBDA developed in Ssemujju et al. (2026) directly to the IFS data allowed grid point detection of LBF passages and direct comparison with the passage at a large network of weather observations. The main findings are:

- The results demonstrate that the IFS provides a plausible representation of the regional-scale lake-breeze circulation. However, compared with automatic weather stations, IFS overestimates the frequency of LBF passages by ~26% and exhibits an early-arrival bias of 1–2 h.
- Evaluation of three commonly used proxy diagnostics against OLBDA-identified LBFs (based on wind, temperature, and dew point, as shown in Figure 2) indicates that the BLH gradient provides the most consistent and physically interpretable representation of LBF structure. The specific humidity gradient performs nearly as well, particularly during the early-to-mid afternoon, while horizontal convergence was found to be a rather inadequate proxy in our case due to the high level of noise and low level of coherence.

- Vertical cross-sections show a well-defined LBC along both western and northern transects, with marked differences in strength and depth. The western transect, favorably aligned with the prevailing easterly synoptic flow, exhibits stronger low-level convergence, deeper ascent, and greater inland penetration (~200 km), whereas the northern transect shows a weaker, shallower circulation. Furthermore, the results show that inland regions often develop a deep (~3 km) convective boundary layer prior to frontal passage, with a distinct BLH gradient marking the ascent zone, consistent with density-current-like LBF structure.

Overall, our results suggest that ECMWF IFS 9-km operational analyses provide a plausible and coherent picture of daytime evolution of the three-dimensional land-lake circulation at the western and northern shores of Lake Victoria during the dry seasons. Some deficiencies are noted regarding the overestimation of the frequency and swifter inland propagation. The tendency of the IFS to predict more LBFs and earlier frontal arrival times may be due to biases in the representation of land-lake thermal contrasts, surface heat fluxes, boundary-layer evolution, shoreline roughness transitions, and limitations in the representation of turbulent mixing, which require further investigation.

The superior performance of the BLH and specific humidity gradients compared to surface convergence likely reflects the thermodynamic nature of the LBF, which separates relatively cool, moist marine air from warmer continental air and thereby produces sharp horizontal contrasts in moisture and boundary-layer structure that closely delineate the frontal position (e.g., Simpson 1994; Miller et al. 2003). As the front propagates inland, strong gradients in specific humidity and BLH remain closely aligned with its leading edge, providing spatially coherent markers of frontal location. By contrast, surface convergence is often diffused or displaced from the thermodynamic boundary and can be modified by local topography and mesoscale circulations, making it a less reliable standalone indicator of LBF position.

According to IFS, the depth of the LLB reaches about 3–4 km (Figure 4). The northern transect in Figure 4 covers Entebbe at the lakeshore. Fraedrich (1968) utilized two seasons of PIBAL balloon wind soundings from Entebbe, but only up to 1920 m. His results indicate that in June–August, the depth of the LLB at the coast of Entebbe in the afternoon (12–18 LT) is 1920 m or higher, while it is shallower in December–February. Similar seasonal differences were evident in IFS (not shown). Our NW-SE transect is similar to the one discussed in Woodhams et al. (2019), using Met Office Unified Model convection-permitting simulations at 1.5 km resolution. From comparing our Figure 4f with Fig. 7n in Woodhams et al. (2019), it can be seen that upward motion at the LBF reached around 600 hPa. Unfortunately, no upper-air observations at some distances away from the coast are available to investigate the vertical extent of the LLB.

Our results suggest that IFS analysis can be used to study the LLB and as boundary conditions to drive higher resolution atmospheric models, including those that simulate atmospheric chemistry and pollution. A caveat for long-term climatologies is that IFS operational analyses are inhomogeneous due to changes in the model physics in the different model cycles (ECMWF 2025). Yet, the next ECMWF reanalysis, ERA6 (https://climate.copernicus.eu/copernicus-climates-era6-reanalysis-production-starts), planned to be released in 2027 at 14 km resolution, that is, more than double the resolution of ERA5 (32 km), could solve this issue. Other high-resolution global, like DWD ICON DREAM at 13 km (Valmassoi et al. 2025), can be used as well to obtain a feeling how differences in data assimilation and model physics impact the LLB. Using these data sets, diurnal, seasonal and interannual variations in the LLB systems of Lake Victoria could be studied. The OBLDA-derived hourly positions of the LLB from weather stations in the period 2017–2022 can also be used to quantitatively assess LLB forecasts that are freely available from both the DWD and ICON model. Furthermore, the findings of this study have implications for the growing use of ECMWF IFS-based reanalysis products as training datasets for AI weather models. Any bias in the representation of lake-breeze circulations may be transferred to data-driven forecasting systems, highlighting the importance of accurately capturing mesoscale boundary-layer processes.

Author Contributions

Musa Ssemujju: conceptualization, methodology, data curation, formal analysis, visualization, investigation, writing – original draft, writing – review and editing, validation, software. **Andreas H. Fink:** supervision, methodology, conceptualization, writing – review and editing, formal analysis, investigation. **Marlon Maranan:** conceptualization, methodology, investigation, writing – review and editing, formal analysis, supervision. **Simon Ageet:** methodology, writing – review and editing, formal analysis, investigation.

Acknowledgments

We thank the European Centre for Medium-Range Weather Forecasts (ECMWF) for granting us access to the forecast and analysis products. We also thank the Trans-African Hydro-Meteorological Observatory (TAHMO) and Uganda Department of Meteorological Services (UDMS) for providing the AWS data used in this study. M.S. greatly appreciates the financial support provided by the German government through the DAAD PhD Fellowship Programme. Open Access funding enabled and organized by Projekt DEAL.

Funding

The authors have nothing to report.

Conflicts of Interest

The authors declare no conflicts of interest.

Data Availability Statement

The ECMWF IFS operational analysis data used are available through the ECMWF operational archive (https://www.ecmwf.int/en/forecasts/access-forecasts/access-archive-datasets). The automatic weather station data were obtained from two sources, (i.e., TAHMO and UDMS) and are not publicly available. For more information about TAHMO data, please visit https://tahmo.org/climate-data/. Data from UDMS stations can be obtained from UDMS upon request. The satellite imagery data are freely available and were accessed from NASA EOSDIS Worldview at https://worldview.earth data.nasa.gov/. The algorithm developed and other code used in this study are currently not available through a public repository but can be directly accessed from the first author upon request. However, the authors intend to make the code publicly available on a GitHub repository after completion of necessary documentation and licensing arrangements. Information of repository and licensing will be provided upon final public release.

References

Antonelli, M., and R. Rotunno. 2007. "Large-Eddy Simulation of the Onset of the Sea Breeze." *Journal of the Atmospheric Sciences* 64, no. 12: 4445–4457. https://doi.org/10.1175/2007jas2261.1.

Anyah, R. O., F. H. M. Semazzi, and L. Xie. 2006. "Simulated Physical Mechanisms Associated With Climate Variability Over Lake Victoria Basin in East Africa." *Monthly Weather Review* 134, no. 12: 3588–3609. https://doi.org/10.1175/mwr3266.1.

Borne, K., D. Chen, and M. Nunez. 1998. "A Method for Finding Sea Breeze Days Under Stable Synoptic Conditions and Its Application to the Swedish West Coast." *International Journal of Climatology* 18, no. 8: 901–914. https://doi.org/10.1002/(sici)1097-0088(19980630)18:8<901::aid-joc295>3.3.co;2-6.

Brown, A., C. Vincent, and E. Short. 2026. "Identifying Sea Breezes From Atmospheric Model Output (sea_breeze v1.1)." *Geoscientific Model Development* 19, no. 2: 933–953. https://doi.org/10.5194/gmd-19-933-2026.

Chamberlain, J. M., C. L. Bain, D. F. A. Boyd, K. McCourt, T. Butcher, and S. Palmer. 2014. "Forecasting Storms Over Lake Victoria Using a High Resolution Model." *Meteorological Applications* 21, no. 2: 419–430. https://doi.org/10.1002/met.1403.

Crosman, E. T., and J. D. Horel. 2010. "Sea and Lake Breezes: A Review of Numerical Studies." *Boundary-Layer Meteorology* 137, no. 1: 1–29. https://doi.org/10.1007/s10546-010-9517-9.

Drobinski, P., S. Bastin, A. Dabas, P. Delville, and O. Reitebuch. 2006. "Variability of Three-Dimensional Sea Breeze Structure in Southern France: Observations and Evaluation of Empirical Scaling Laws." *Annales Geophysicae* 24, no. 7: 1783–1799. https://doi.org/10.5194/angeo-24-1783-2006.

ECMWF. 2016. "Implementation of IFS Cycle 41r2, Reading, UK." https://confluence.ecmwf.int/display/FCST/Implementation+of+IFS+Cycle+41r2.

ECMWF. 2017. "Implementation of IFS Cycle 43r1, Reading, UK." https://confluence.ecmwf.int/display/FCST/Implementation+of+IFS+Cycle+43r1.

ECMWF. 2019. "Implementation of IFS Cycle 45r1, Reading, UK." https://confluence.ecmwf.int/display/FCST/Implementation+of+IFS+Cycle+45r1.

ECMWF. 2020. "Implementation of IFS Cycle 46r1, Reading, UK." https://confluence.ecmwf.int/display/FCST/Implementation+of+IFS+Cycle+46r1.

ECMWF. 2022. "Implementation of IFS Cycle 47r1, Reading, UK." https://confluence.ecmwf.int/display/FCST/Implementation+of+IFS+Cycle+47r1.

ECMWF. 2025. "Integrated Forecasting System (IFS) Cycles Overview. European Centre for Medium-Range Weather Forecasts." https://www.ecmwf.int/en/forecasts/documentation-and-support/changes-ecmwf-model.

Finney, D. L., J. H. Marsham, D. P. Rowell, et al. 2020. "Effects of Explicit Convection on Future Projections of Mesoscale Circulations, Rainfall, and Rainfall Extremes Over Eastern Africa." *Journal of Climate* 33, no. 7: 2701–2718. https://doi.org/10.1175/jcli-d-19-0328.1.

Flohn, H., and K. Fraedrich. 1966. "Tagesperiodische Zirkulation und Niederschlagsverteilung am Victoria-See (Ostafrika) (The Daily Periodic Circulation and Distribution of Rainfall Over Lake Victoria, in German)." *Meteorologische Rundschau* 19: 157–165.

Fraedrich, K. 1968. "Das Land- Und Seewindsystem Des Victoria-Sees Nach Aerologischen Daten (The Land and Lake Breeze System of Lake Victoria Based on Aerological Data, in German)." *Archiv Für Meteorologie, Geophysik Und Bioklimatologie, Serie A* 17, no. 2–3: 186–206. https://doi.org/10.1007/bf02247084.

Fu, S., R. Rotunno, J. Chen, X. Deng, and H. Xue. 2021. "A Large-Eddy Simulation Study of Deep-Convection Initiation Through the Collision of Two Sea-Breeze Fronts." *Atmospheric Chemistry and Physics* 21, no. 12: 9289–9308. https://doi.org/10.5194/acp-21-9289-2021.

Hannak, L., P. Knippertz, A. H. Fink, A. Kniffka, and G. Pante. 2017. "Why Do Global Climate Models Struggle to Represent Low-Level Clouds in the West African Summer Monsoon?" *Journal of Climate* 30, no. 5: 1665–1687. https://doi.org/10.1175/jcli-d-16-0451.1.

Hersbach, H., B. Bell, P. Berrisford, et al. 2020. "The ERA5 Global Reanalysis." *Quarterly Journal of the Royal Meteorological Society* 146, no. 730: 1999–2049. https://doi.org/10.1002/qj.3803.

Holtslag, A. A. M., G. Svensson, P. Baas, et al. 2013. "Stable Atmospheric Boundary Layers and Diurnal Cycles: Challenges for Weather and Climate Models." *Bulletin of the American Meteorological Society* 94, no. 11: 1691–1706. https://doi.org/10.1175/bams-d-11-00187.1.

Kalthoff, N., B. Adler, and I. Bischoff-Gauss. 2020. "Spatio-Temporal Structure of the Boundary Layer Under the Impact of Mountain Waves." *Meteorologische Zeitschrift* 29, no. 5: 409–424. https://doi.org/10.1127/metz/2020/1033.

Laird, N. F., D. A. R. Kristovich, X.-Z. Liang, R. W. Arritt, and K. Labas. 2001. "Lake Michigan Lake Breezes: Climatology, Local Forcing, and Synoptic Environment." *Journal of Applied Meteorology* 40, no. 3: 409–424. https://doi.org/10.1175/1520-0450(2001)040<0409:lmlbcl>2.0.co;2.

Markowski, P., and Y. Richardson. 2010. *Mesoscale Meteorology in Midlatitudes*. John Wiley & Sons.

May, R. M., S. C. Arms, P. Marsh, et al. 2019. "MetPy: A Python Package for Meteorological Data. UCAR/NSF Unidata [Code]." https://www.unidata.ucar.edu/software/metpy/.

Miller, S. T. K., B. D. Keim, R. W. Talbot, and H. Mao. 2003. "Sea Breeze: Structure, Forecasting, and Impacts." *Reviews of Geophysics* 41, no. 3: 1011. https://doi.org/10.1029/2003rg000124.

Papanastasiou, D. K., and D. Melas. 2009. "Climatology and Impact on Air Quality of Sea Breeze in an Urban Coastal Environment." *International Journal of Climatology* 29, no. 2: 305–315. https://doi.org/10.1002/joc.1707.

Savazzi, A. C. M., L. Nuijens, I. Sandu, G. George, and P. Bechtold. 2022. "The Representation of the Trade Winds in ECMWF Forecasts and Reanalyses During EUREC^{4}A." *Atmospheric Chemistry and Physics* 22, no. 19: 13049–13066. https://doi.org/10.5194/acp-22-13049-2022.

Sills, D. M. L., J. R. Brook, I. Levy, P. A. Makar, J. Zhang, and P. A. Taylor. 2011. "Lake Breezes in the Southern Great Lakes Region and Their Influence During BAQS-Met 2007." *Atmospheric Chemistry and Physics* 11, no. 15: 7955–7973. https://doi.org/10.5194/acp-11-7955-2011.

Simpson, J. E. 1994. *Sea Breeze and Local Winds*, 234. Cambridge University Press.

Ssemujju, M., M. Maranan, A. H. Fink, and S. Ageet. 2026. "A Novel Algorithm for Detecting Lake-Breeze Fronts at Lake Victoria Using Station Observations." *Journal of Applied Meteorology and Climatology* 65: 941–960. https://doi.org/10.1175/jamc-d-25-0253.1.

Stull, R. B. 1988. *An Introduction to Boundary Layer Meteorology*. Springer Science & Business Media.

Thiery, W., E. L. Davin, H.-J. Panitz, M. Demuzere, S. Lhermitte, and N. van Lipzig. 2015. "The Impact of the African Great Lakes on the Regional Climate." *Journal of Climate* 28, no. 10: 4061–4085. https://doi.org/10.1175/jcli-d-14-00565.1.

Thiery, W., E. L. Davin, S. I. Seneviratne, K. Bedka, S. Lhermitte, and N. P. M. van Lipzig. 2016. "Hazardous Thunderstorm Intensification Over Lake Victoria." *Nature Communications* 7: 12786. https://doi.org/10.1038/ncomms12786.

Valmassoi, A., H. Anlauf, A. Becker, et al. 2025. "ICON-DREAM: ICON-Dual resolution Reanalysis for Emulators, Applications and Monitoring (Version v1.0)." Deutscher Wetterdienst (DWD) Climate Data Center (CDC). https://doi.org/10.5676/dwd/icon-dream_v1.

van de Giesen, N., R. Hut, and J. Selker. 2014. "The Trans-African Hydro-Meteorological Observatory (TAHMO)." *Wiley Interdisciplinary Reviews: Water* 1, no. 4: 341–348. https://doi.org/10.1002/wat2.1034.

Van de Walle, J., W. Thiery, O. Brousse, N. Souverijns, M. Demuzere, and N. P. M. van Lipzig. 2020. "A Convection-Permitting Model for the Lake Victoria Basin: Evaluation and Insight Into the Mesoscale Versus Synoptic Atmospheric Dynamics." *Climate Dynamics* 54, no. 3–4: 1779–1799. https://doi.org/10.1007/s00382-019-05088-2.

Virts, K. S., and S. J. Goodman. 2020. "Prolific Lightning and Thunderstorm Initiation Over the Lake Victoria Basin in East Africa." *Monthly Weather Review* 148: 1971–1985. https://doi.org/10.1175/mwr-d-19-0260.1.

Woodhams, B. J., P. A. Barrett, J. H. Marsham, et al. 2022. "Aircraft Observations and Sub-Km Modelling of the Lake–Land Breeze Circulation Over Lake Victoria." *Quarterly Journal of the Royal Meteorological Society* 148, no. 743: 557–580. https://doi.org/10.1002/qj.4155.

Woodhams, B. J., C. E. Birch, J. H. Marsham, T. P. Lane, C. L. Bain, and S. Webster. 2019. "Identifying Key Controls on Storm Formation Over the Lake Victoria Basin." *Monthly Weather Review* 147, no. 9: 3365–3390. https://doi.org/10.1175/mwr-d-19-0069.1.

Zhu, M., and B. W. Atkinson. 2004. "Observed and Modelled Climatology of the Land–Sea Breeze Circulation Over the Persian Gulf." *International Journal of Climatology* 24, no. 7: 883–905. https://doi.org/10.1002/joc.1045.

Supporting Information

Additional supporting information can be found online in the Supporting Information section. **Figure S1:** Two-dimensional histogram comparing lake-breeze front arrival hours identified from AWS observations (*x*-axis) and the ECMWF IFS analysis (*y*-axis) for all common lake-breeze events across the station network. The red dashed line denotes perfect agreement. The concentration of events on and immediately below the 1:1 line indicates that, while the IFS generally captures the timing of lake-breeze arrivals, it exhibits a systematic tendency to predict the arrival approximately 1 h earlier than observed.